

Evaluation of ULS Bathymetry for Hydrodynamic Modelling

Joseph C. Haines¹, Maria V. Peppas¹, Christos Iliadis¹, Jon P. Mills¹, Vassilis Glenis¹, Gottfried Mandlbürger²

¹ School of Engineering, Newcastle University, Newcastle, NE1 7RU, UK –
(j.c.haines, maria-valasia.peppas, chris.ilias, jon.mills, vassilis.glenis)@newcastle.ac.uk

² Dept. of Geodesy and Geoinformation, TU Wien, Vienna, 1040, Austria – gottfried.mandlbuerger@geo.tuwien.ac.at

Keywords: Topo-bathymetric Laser Scanning, Hydrodynamic Modelling, Bathymetric Flood Modelling, Unmanned Laser Scanning, Bathymetric Surveying, Digital Terrain Models.

Abstract

The importance of accurate and reliable DTMs are paramount for hydrodynamic modelling. Currently, bathymetry is either not considered or a simpler mathematical representation of the river is created from observed cross sections for hydrodynamic models. Topographic and Bathymetric LiDAR creates centimetre resolution bathymetry and topography. However, it has not been applied into large scale hydrodynamic modelling. Following a major flood event in September 2024, a large fieldwork campaign on the Pielach River, Lower Austria, was conducted to capture the environmental changes using Topographic-Bathymetric LiDAR. Metre resolution DTMs of the bathymetric and topographic environment were created to produce flood inundation maps from crewed and uncrewed aerial mapping systems. Using the observed flow data of the September 2024 storm, resulting flood models prove the inclusion of bathymetry can produce reliable flood models with depths of greater than 6 m modelled. Due to the lower flying altitude and tactical flight paths of ULSs, it is possible to identify regions occluded by vegetation that would otherwise be overlooked by crewed Airborne Laser Scanning methods to produce more reliable flood models.

1. Introduction

1.1 Background

Accurate Digital Terrain Models (DTMs) are fundamental in hydrodynamic modelling to determine the flow of water through a region or catchment (Cook and Merwade, 2009). Creating a DTM with only topography is well documented and such DTMs are widely used for hydrodynamic modelling (Bangen et al., 2014; Cook and Merwade, 2009; Glenis et al., 2018; Horritt and Bates, 2002; Tomsett and Leyland, 2019). The bathymetric environment is rarely considered within the DTM for two main reasons (Guo et al., 2021). Firstly, it is difficult to georeference multiple datasets into a single DTM (Janowski et al., 2024). Secondly, it is computationally simpler to assume a mathematically derived channel or water surface model rather than implement an all-encompassing topographic-bathymetric DTM (Grimaldi et al., 2018).

However, it is possible to survey the river bathymetry to

produce centimetre-resolution point clouds (Grimaldi et al., 2018; Janowski et al., 2024; Kasvi et al., 2019; Mandlbürger et al., 2020, 2016; Woodget et al., 2015). Bathymetric surveying techniques including Sound Navigation and Ranging, photogrammetry and traditional methods including GNSS and total station observations can be employed to provide sub-metre resolution datasets (Brasington et al., 2003; Cook and Merwade, 2009; Janowski et al., 2024). Although these techniques produce a geospatial representation of the bathymetry, there are limitations including spatial coverage, depth penetration, observation time and additional geospatial transformations for combining multiple datasets.

Topographic and Bathymetric Light Detection and Ranging (Topo-bathy LiDAR) is a unique technique where green wavelength pulses ($\lambda = 532$ nm) are emitted, penetrate water to observe the topographical and bathymetric environments simultaneously (Mandlbürger et al., 2020). Mounted on crewed aircraft (Airborne Laser Scanning, ALS) and uncrewed aerial vehicles (UAV-borne Laser Scanning, ULS), large areas are

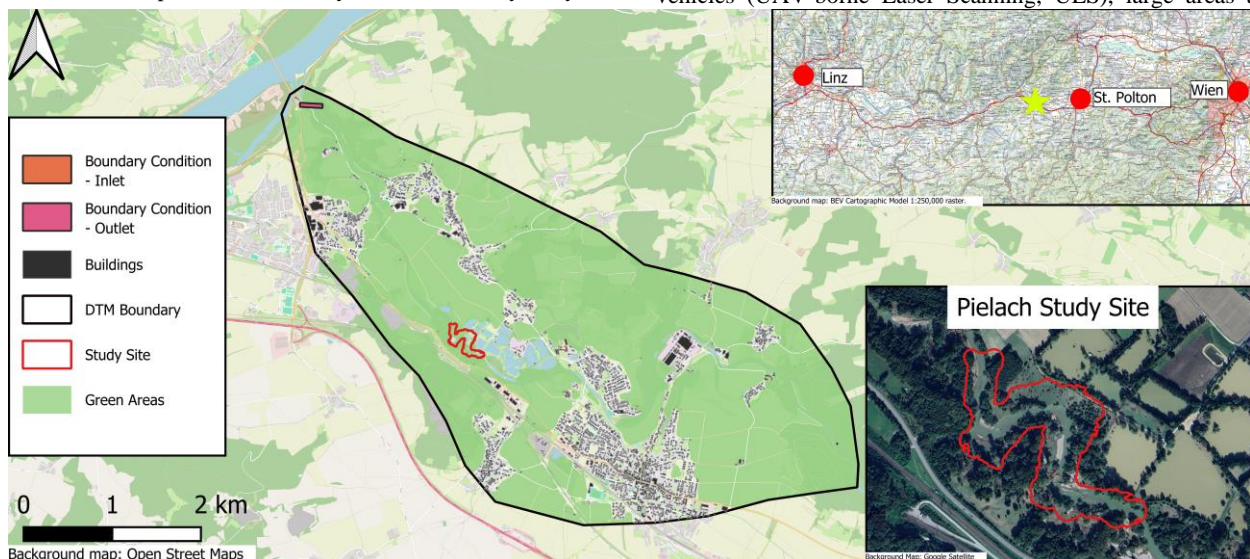


Figure 1: Overview of the study region, Pielach River, Austria

surveyed in a short timeframe whilst obtaining centimetre resolution point clouds. Using this technique, there are no requirements for multiple datasets or additional georeferencing transformations.

Once a bathymetric and topographic DTM (DTM-W) is created, there are various hydrodynamic models used to predict flooding by solving the shallow water equations including *LIS FLOOD*, *FloodMap* and *CityCAT* (Guo et al., 2021). *CityCAT* is such a model that has been developed within Newcastle University and is available for use and further development (Glenis et al., 2018; Iliadis et al., 2023).

1.2 Aim of Research

Current research suggests that although Topo-bathy LiDAR is widely used, there have been limited investigations using Topo-bathy LiDAR for hydrodynamic modelling on large scale extents (Frizzle et al., 2024; Mandlbürger et al., 2015; McKean et al., 2014). This research investigates the impacts of using centimetre resolution DTM-Ws created from Topo-bathy LiDAR to predict flood extents of a region of the Pielach River using *CityCAT* hydrodynamic model. To highlight the impact of bathymetry, an initial topographic DTM with no bathymetry will be considered as a baseline model for the Pielach catchment. Following this, ALS and ULS derived bathymetry of a region of the Pielach River will be embedded in the catchment model where differences between DTM-Ws will be examined.

2. Methodology

2.1 Site Location

For this study, a pre-alpine region of the Pielach River, Austria was investigated (N 48°12'50", E 15°22'30", WGS84) (Figure 1). This region has been extensively researched, recently following a major flood event in September 2024 where 250 mm of rainfall over six days resulted in 27 deaths (Blöschl, 2024; ECMWF, 2024; Mandlbürger et al., 2025). Due to the extensive research and the recent flood event, this is an ideal location to determine the suitability of ULS Topo-bathy ULS for hydrodynamic modelling (Mandlbürger et al., 2025, 2020, 2016; Wieser et al., 2016; Wimmer et al., 2024).

The study site covers 100,857 m² and includes different fluvial features including meanders, gravel beds, riparian forests and surrounding pastures (Figure 1). A full description of the environment is outlined in Mandlbürger *et al.*, (2015) however, due to recent flooding, various characteristics have morphed.

2.2 Field Campaign

Data collection was undertaken between 9th and 24th October 2025 using the *RIEGL VQ-880-GII* ALS and a ULS mounted *RIEGL VQ-840-GL* Topo-bathy LiDAR sensors. A comprehensive overview of the survey methodology is provided by Mandlbürger *et al.*, (2025). A summary of the field campaign is provided below.

Both LiDAR sensors operate with a green wavelength (532 nm) pulse to allow water penetration. Each sensor creates a point cloud of the topography and bathymetry but operate slightly differently. The *VQ-840-GL* has a lateral Field of View (FoV) of $\pm 20^\circ$ and $\pm 14^\circ$ in the flying direction (*RIEGL Laser Measurement Systems*, 2024). Based on a 200 kHz pulse repetition rate, a theoretical maximum water depth penetration

of 1.7 Secchi depth can be obtained from a 75 m flying altitude (*RIEGL Laser Measurement Systems*, 2024). Data was obtained using pairs of flight lines to observe each bank side. Additional cross-strips were obtained at meanders to obtain complete coverage.

The *VQ-880-GII* has different parameters due to the higher-flying altitude. The FoV in all direction is $\pm 20^\circ$ and can operate with a pulse repetition rate of up to 700 kHz (*RIEGL Laser Measurement Systems*, 2025). Therefore, when flying at approximately 650 m, a maximum water depth penetration of 2.0 Secchi depth can be obtained (*RIEGL Laser Measurement Systems*, 2025). A similar flying pattern to the ULS acquisition was used where pairs of flight lines were used to obtain full coverage. Overlapping lines were obtained to assist in the georeferencing stage. Due to the flying altitude, strategic flight paths would not be possible.

Each sensor will produce a point cloud. As the ALS sensor is mounted on an aircraft, the resulting point cloud will cover a broader area. The ULS surveys a smaller region at a lower altitude to maintain visual line of sight due to ULS flying regulations (European Union Aviation Safety Agency, 2024). As the ULS must be flown at a lower altitude, multiple flight lines are required for complete coverage. However, the lower flying altitude of the ULS system will, theoretically, produce a point cloud with a greater spatial resolution. Both sensors face difficulty with vegetation causing occlusions therefore missing ground and riverbed data. Topo-bathy LiDAR has generally the same properties as traditional LiDAR and can penetrate vegetation (Kraus and Pfeifer, 1998; Wieser et al., 2016). Due to the flying altitude of the ALS system, thick vegetation, and tall trees, laser pulses may not reach the ground surface. As the ULS flies at a lower altitude, pulses are more likely to reach ground level. To aid this, strategic flight paths were conducted to provide additional bathymetric data where ALS may miss features.

Both resulting point clouds require to be georeferenced which can be conducted using onboard GNSS and Inertial Measuring Units (IMU). To aid this, Ground Control Points (GCPs) were distributed across the survey area to aid this. GNSS observations were made between 1.5 to 5.5 hours and post-processed to a local GNSS base station in the village of Loosdorf less than 2 Km away (Mandlbürger et al., 2025).

Although GCPs and onboard GNSS and IMU measurements can create a co-ordinated point cloud, further field measurements are required to ensure high accuracy in the resulting georeferenced datasets. Eight sloped planes were installed and surveyed using a *Leica MS60* total station. These planes are used to georeference the ALS and ULS datasets to the local coordinate system (ETRS89/UTM 33N). Furthermore, 18 cross sections were observed using a *Leica MS60* total station with a pogo mounted 360° prism at approximately 1 m intervals across the watercourse to assist in data verification.

2.3 DTM Generation

Creating DTMs was undertaken using *OPALS* (Orientation and Processing of Airborne Laser Scanning data) point cloud software to examine and extract information from each point clouds (Pfeifer et al., 2014). In this instance, slightly different methodologies were required to process each dataset. The ULS point cloud used the *StripAdjust* module to georeference each strip to each other and GCPs to transform point clouds to ETRS89 UTM 33N (Glira et al., 2016). Following this, the

refraction correction was applied to the bathymetric points. This required a water surface model to be generated, calculation of beam vectors and application of correct refraction constants using the *Snellius* module (Mandlbürger et al., 2013). Two refraction constants were applied to the below water points: 1.33 for deflection and 1.35 for beam velocity.

As the study site is heavily vegetated, the *TerrainFilter* module was employed to extract ground features from vegetation and noise (Kraus and Pfeifer, 1998; Shan and Toth, 2018). Multiple iterations and filters were required to ensure only ground features remained. Due to the dense vegetation, gaps appear in the DTM. Smaller gaps would be filled by interpolation, while larger one would be left unfilled.

The ALS post processing follows the same procedure however, initial georeferencing was conducted by the scanners manufacturer's software *RiPROCESS*. After strip adjustment, the resulting strip point clouds underwent standard quality assessment using the *opalsQuality* script to ensure correct strip alignment and georeferencing (Opals, 2025).

Hydrodynamic modelling can be performed using the ALS and ULS DTMs however, results are limited to the extents of the surveyed area. To address this, a 1 m resolution DTM covering the entire Pielach catchment (~ 54 km²) was provided by the Federal Office of Metrology and Surveying (BEV). The BEV DTM, while suitable for hydrodynamic modelling, does not contain any bathymetric information.

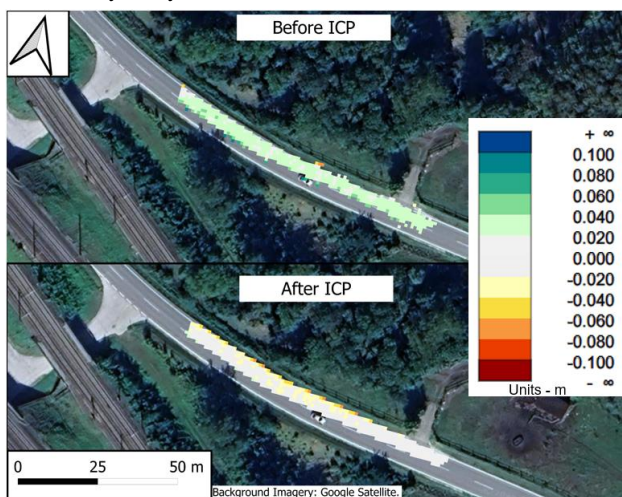


Figure 2: One example among all road regions used for *ICP* transformation.

Using *OPALS*, it was possible to combine the BEV DTM with each DTM to produce a comprehensive DTM for the Pielach catchment. Both ULS and ALS DTMs were co-registered to the BEV DTM using the Iterative Closest Point (*ICP*) module in *OPALS* to minimise differences and merged into the BEV DTM (Glira et al., 2015). Applying *ICP* proved difficult due to survey area consisting mainly of vegetation and temporal changes in land use between data acquisitions. Data collection for the BEV DTM has not been documented. To conduct *ICP* between BEV and ALS DTMs, only major roads were used (Figure 2).

ICP proved difficult between the transformed ALS and the ULS DTMs. Most of the environment is vegetation which continuously changes. Due to absence of fixed features and the dynamic nature of the environment, achieving an accurate and precise *ICP* transformation was challenging. To conduct *ICP*, similar features had to be determined by an initial height

comparison. Only open flat areas with an elevation difference less than 10 cm between ALS and ULS DTMs were identified and used.

After applying the *ICP* transformation, the bathymetry and the adjacent 10 m of topography from the ALS and ULS DTMs were used to replace the BEV data in overlapping areas. To reduce computational time, DTMs were further clipped to regions where water flow is expected, based on a watershed analysis performed in *ArcGIS Pro*. Further filtering was employed to remove points significantly above the level of the initial boundary condition. In summary, three DTMs were created for hydrodynamic modelling with 1 m spatial resolution: BEV only, BEV merged with ALS (BEVALS) and, BEV merged with ULS (BEVULS).

2.4 Hydrodynamic Modelling

CityCAT simulations required a high-powered server. A *Blades* server was used consisting of two *Intel® Xeon® Gold 6134 CPU @ 3.20GHz* processors with 767 GB of RAM. The system runs a 64-bit operating system with a x64-based processor. To create a hydrodynamic model, river flow measurements are required and are provided by the Office of the Lower Austrian State Government. Due to the scale of the flood event, only a daily average was provided due to flood water causing damage at gauging stations Großsiering and Hofstetten.

Flow is one of the parameters *CityCAT* requires (Glenis et al., 2018). Parameters are controlled through a configuration file where constants are stored, and model conditions are determined. Simulation length was 23-hours with flood maps produced every 30 minutes. Friction coefficients were determined using Manning's Coefficients of Friction (Chow, 2009). Hydraulic conductivity, wetting front suction head, effective porosity and effective saturation constants were determined based on the Green-Ampt parameters using the Brooks-Corey equation (D. L. Brakensiek et al., 1981). Based on the soil type within the Pielach catchment, suitable constants were applied (Chow et al., 1988; Rawls et al., 1983).

To apply water flow, boundary conditions are required to determine the inflow and outflow of water. Boundary conditions are generated as a polygon and converted to ASCII format. Buildings and green areas were identified to apply friction coefficients and surface permeability constants. These were created as polygons and converted to ASCII format.

Initial experiments used a DTM limited to the study site (Figure 1). As the area is fully vegetated, no green area or buildings footprints were required. Therefore, a single friction coefficient and infiltration rate for initial experiments were used. For the full catchment, building footprints and green areas had to be determined. Building footprints were obtained from *Overture Maps* (Overture Maps Foundation, 2024). Green areas were initially extracted using Sentinel-2 Land Cover dataset hosted by *ESRI* and produced by *European Space Agency* (The European Space Agency, 2025). However, due to the 10 m resolution, features including roads, railways and footpaths were overlooked. Transport routes were provided by BEV from the Digital Landscape Model – Traffic dataset. Each transport route in the region was extracted, a 10 m buffer applied around each route, and removed from conflicting green spaces.

Once each model was set up, numerous experiments were carried out to optimise *CityCAT*. Initial experiments used the ALS DTM with low flow values over a small-time event before

increasing the scale of the event for subsequent experiments. Due to the high spatial resolution of the DTMs, each model required calibration of the boundary conditions. Where the boundary is too small, a mass of water will build up in that area therefore causing a delay in the flow of water. If the boundary is set too large, incorrect regions may be flooded.

To highlight the benefits of ULS derived bathymetry, each DTM-W was evaluated under identical flow conditions. In theory, incorporating ALS bathymetry should yield more detailed results than the BEV DTM. However, ULS bathymetry is expected to offer more comprehensive results and insights particularly in areas where ALS data is limited or unavailable.

3. Results

3.1 DTM Results

The quality assessment confirmed successful georeferencing of the ALS point cloud with an error of $2 \text{ mm} \pm 24 \text{ mm}$ and spatial resolution of $\sim 0.6 \text{ m}$. The ULS had improved georeferencing results with an error of $2 \text{ mm} \pm 11 \text{ mm}$ and spatial resolution of $\sim 10 \text{ cm}$. Vertical comparisons between each DTM and observed cross sections are provided in Table 1. Although the difference of the ALS is lower than ULS, the standard deviation and spread of the ULS is much lower. This suggests the ULS data may be prone to a larger bias however will be more precise. The reason for the large ALS deviations is due to data capture. The ALS data was observed on 9th October whereas the section and ULS data was obtained on 24th October. Therefore, the differences are likely caused by the natural variation of the river between campaigns. Following further inspection of the cross sections, both datasets are suitable for further analysis.

Prior to *ICP* application, the BEV and ALS DTMs showed an initial elevation difference of $0.12 \text{ m} \pm 0.549 \text{ m}$ across the study area. However, due to the region's dense vegetation and the differences in bathymetric representation, these differences may not be fully reliable. To better assess alignment, roads common to both datasets were compared. After five *ICP* iterations, the differences were reduced from $17 \text{ mm} \pm 86 \text{ mm}$ to $3 \text{ mm} \pm 19 \text{ mm}$ (Figure 2). This transformation was then applied to the full ALS DTM and validated before further use.

For the ULS and ALS transformation, 14 iterations were required to produce a suitable *ICP* transformation. Initial

comparisons produced a difference of $59 \text{ mm} \pm 153 \text{ mm}$. Due to the terrain and the time between surveys, best results produced a mean difference of $32 \text{ mm} \pm 22 \text{ mm}$. Visual inspection revealed a consistent bias and corrected through a vertical alignment. Once the transformations were applied, each dataset was checked prior to use. Variation in bathymetric representations and conditions between each DTM are illustrated in Figure 3.

	ULS	ALS
Mean (m)	-0.020	-0.008
Std. Dev. (m)	0.016	0.041
Max. (m)	0.035	0.117
Min. (m)	-0.079	-0.321

Table 1: Comparison of traditional and aerial bathymetric cross sections. Positive values occur where aerial elevations are greater than traditional elevations.

3.2 Hydrodynamic Results

Due to the high spatial resolution DTM-Ws used and the large flows of the storm event, flood modelling was computationally expensive. Over three weeks of continuous processing, only 5 hours of simulated flow was possible therefore, analysis was restricted to this period.

Initial models were focused on the survey area only. Increasing the flow level produced greater water depths. However once water reaches the extent of the DTM-W, it flows out of the region. Although the flow of water can be seen, the simulated flood depths and extents are inaccurate as water does not reach an adjacent dry region.

Each DTM-Ws created produced flood maps of the entire Pielach catchment using September 2024 storm flows. Figure 4c shows the extent of the flood water from the BEVULS 5 hours into the simulated event. Although this is focused on the Pielach region, the inclusion of bathymetry can create flood models without the need to define the river.

After 150 minutes, BEV produced a maximum water depth of 3.729 m, increases by 11 cm using the BEVALS and depths greater than 4 m were produced by the BEVULS. After five hours of simulation, all three DTM-Ws produced a maximum water depth of 6.75 m.

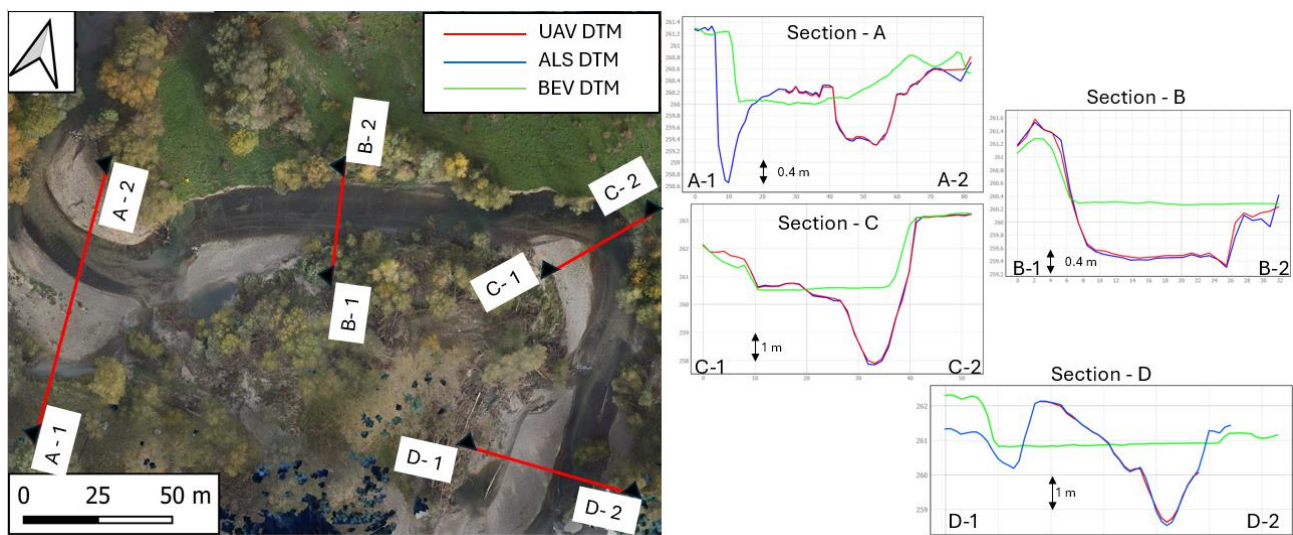


Figure 3: Cross sections of ALS, ULS and BEV DTM-W within the study region. Ortho-mosaic: Mandlbürger et al. (2025).

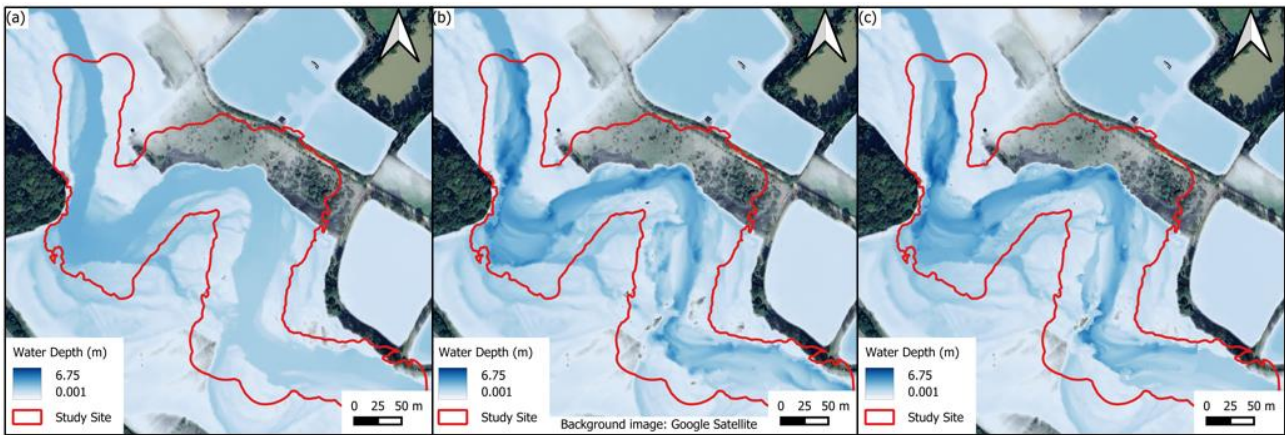


Figure 4: Flood maps at 300 minutes of simulation from BEV (a), BEVALS (b) and BEVULS (c) DTMs.

4. Discussion

Examining the DTM-Ws, the quality of the BEVULS is an improvement compared to the BEVALS. Due to the low flying altitude of the ULS, the resulting point cloud produced a spatial resolution of ~ 10 cm. Compared to ~ 60 cm resolution of the ALS point cloud, the BEVULS was generated using a higher density of ground points, resulting in a more accurate representation. This increased detail enables better noise detection and precise classification.

Figure 5 is an example of the point density differences between ALS and ULS point clouds. Although the terrain can be identified in the ALS (b), the ULS (a) shows the environment in much more detail with a clearer representation of both the topography and the bathymetry. This data can then be used to produce an accurate DTM-W. The ULS point cloud can identify a fallen tree and classified as debris (red circle). Due to the reduced point density of the ALS point cloud, identifying the tree is not possible resulting in inaccurate classification.

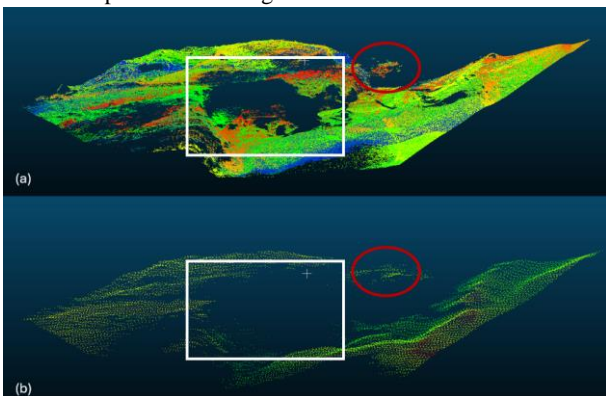


Figure 5: Point cloud of a region surveyed with the ULS sensor (a) and ALS (b).

Figure 5 highlights occlusions in each point cloud (indicated by white squares) caused by tree canopies. In the ULS point cloud, the surrounding environment remains visible and accurately represented, reducing the requirement for large-scale interpolation. The effect of the tree canopies is greater on the ALS point cloud which required more interpolation. This is also present in the topographic environment. Due to the high-flying altitude of the ALS, laser pulses were restricted by the forest to reach ground level. As the ground conditions beneath the tree canopy are unknown, some points may lie on low vegetation rather than actual ground surface. The sparse point density in the ALS point cloud prevents reliable feature classification and

noise detection. In contrast, the lower flight altitude of the ULS system enables greater canopy penetration, allowing more points to reach the ground and produce a more accurate DTM-W. However, ULS limitations arose from the flight path being focused primarily on the river, resulting in limited data coverage within the forest preventing further assessment of ground conditions in those areas.

Thanks to the strategic flight paths and lower altitude of the ULS, a more detailed bathymetric DTM was achieved compared to the ALS. However, the broader spatial coverage of the ALS DTM allowed for the identification of additional terrain features in the surrounding area.

The baseline BEV DTM provided a good flood representation of the catchment. Although bathymetry was not considered in this model, flows followed the river path and areas of flooding could be clearly identified throughout the catchment.

The results further confirm that incorporating bathymetry enables the successful generation of flood maps. Both the BEVALS and BEVULS models accurately simulate the flow through the river channel (Figure 4). This enhanced representation of flood waters is particularly valuable, as it reveals features that may have been previously overlooked. Additionally, the resulting depth maps appear slightly smoother and more refined.

The advantages of using ULS become evident at high flow levels but are even more pronounced during low flow conditions. Figure 6 shows flow conditions in the survey region at 150 (a) and 300 (b) minutes into the simulated event. While both the ALS and ULS capture terrain variations, the greater detail in the ULS point cloud (Figure 5) provides enhanced information on water pathways and flow outputs. During low flow conditions, small features are quickly filled resulting in greater localised water depths within parts of the river channel (Figure 6a). As flows increase (Figure 6b), these regions become fully saturated by the surrounding water.

It should be noted that tributaries and rainfall were not considered in this model. Tributaries were not assigned inflow and rainfall from the storm event was not incorporated. Since bathymetry was only included for the Pielach river, a single inflow boundary condition was defined. Nevertheless, backflow is observed in various tributaries, and the inclusion of rainfall could potentially alter flow patterns and flood depths.

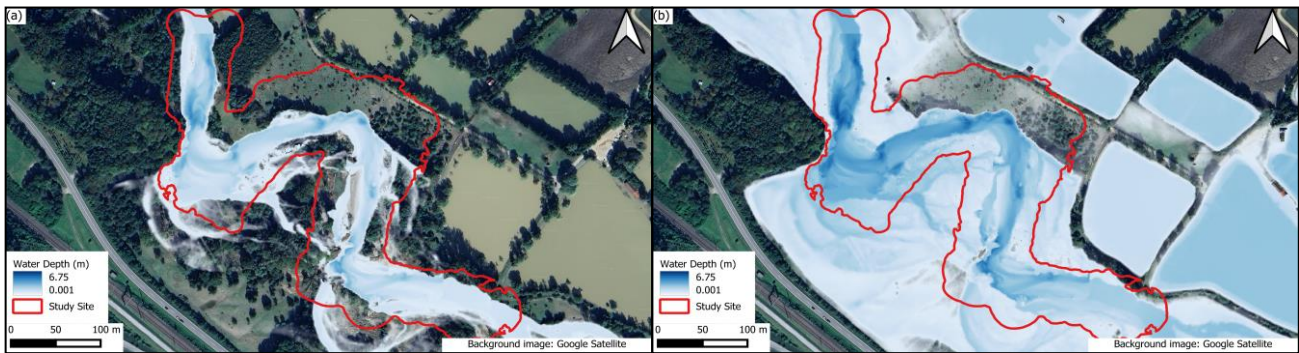


Figure 6: Flood maps from BEVULS DTM at 150 (a) and 300 (b) minutes of simulation.

Differences can be identified between the BEVULS and BEVALS flood models (Figure 4). The inclusion of the ULS bathymetry offers a more accurate representation of the area compared to ALS. While this marks an improvement compared to the BEV DTM, there are still limitations. For example, a smaller secondary additional channel appears in the centre of the study area within the BEVALS but not in BEVULS. This discrepancy arises from the ULS survey being confined to the river channel, whereas the ALS data covers a wider area.

Flood extents also differ between models. When comparing each model at the same timestep (Figure 4) noticeable variations emerge. These differences are primarily due to the inclusion of high-resolution bathymetry. The BEV DTM incorrectly models the flow due to no bathymetry. The BEVALS DTM, based on a sparser point cloud, requires interpolation in areas with significant occlusions, reducing accuracy. In contrast, the ULS data provides a more complete and detailed representation, allowing for more accurate flow modelling.

After 300 minutes of simulation, depth differences between the BEV and BEVALS vary from +3.503 m to -2.266 m (positive values where BEVALS depths are greater than BEV). A mean depth difference of 5 mm ± 91 mm across the catchment is present. As expected, differences are caused by the inclusion of bathymetry and the introduction of fluvial features (Figure 7a). Between the BEVULS and BEVALS flood models, depth differences are +2.816 m to -2.920 m (positive values where BEVULS depths are greater than BEVALS). The average depth

difference is 0 mm ± 53 mm for the entire catchment. As seen in Figure 7b most of the differences occur where vegetation covers riverbanks causing occlusions and unreliable DTM generation. The secondary water channel appears in the BEVALS can also be identified in resulting flood maps.

One challenge lies in the overlapping region between the surveyed and BEV DTMs. In this research, the bathymetry has directly replaced any overlapping BEV data, resulting in a visible step between the datasets. Ideally, this transition zone would be smoothed to produce a seamless connection between the models. However, smoothing was avoided to preserve the natural integrity of the bathymetric data, to evaluate the advantages of ULS Topo-bathy LiDAR. With a larger survey area, the need for smoothing would be reduced making its application more appropriate.

Furthermore, a similar consideration applies to the topographic data. When merging datasets, the bathymetry and the adjacent 10 m buffer area of the topography were merged into the BEV data while the rest of the topography remained unchanged. Since the BEV data is part of a national model, the date and accuracy of the original survey are unknown. As a result, elevation steps may exist in the topographic boundary regions. As with the bathymetry, smoothing could reduce these discontinuities. However, given the limited survey extent, such adjustments could introduce inconsistencies and lead to inaccurate flood maps. This issue could be addressed by incorporating the full extent of the ALS data into the BEV

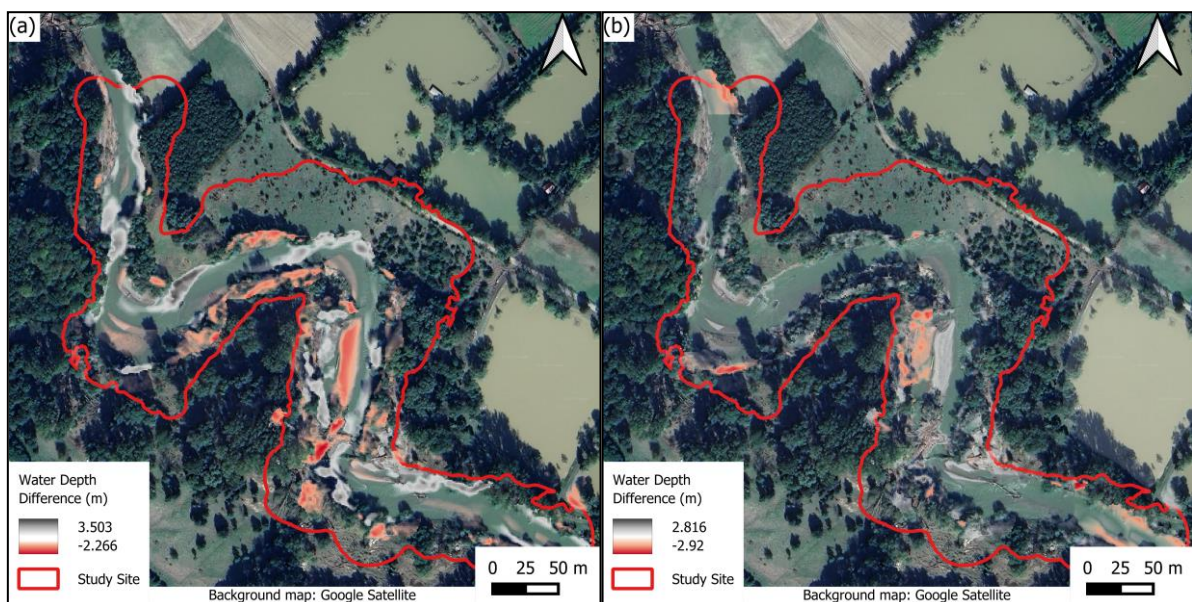


Figure 7: Flood depth differences between BEV and BEVALS (a) and BEVUAV and BEVALS (b) flood maps.

DTM. A future DTM could then be created combining the BEV with the complete ALS dataset with the option to replace the ALS bathymetry with ULS for even greater detail.

A limitation of ULS is spatial coverage. As the flight path of the ULS is focused to the river, little of the surrounding terrain is observed. The ULS DTM revealed features the ALS could not. However, the ALS DTM also captured additional features in areas that were not surveyed by the ULS. Some natural features may have been missed in areas not covered by the ULS survey. To address this, strategic ULS flight paths could be expanded to include the wooded areas nearby. While these regions have already been surveyed using ALS, the higher point density of the ULS data would improve ground classification and enhance detection of features and obstructions.

5. Conclusions

While both ALS and ULS DTM-Ws have their limitations, the advantages of incorporating centimetre resolution bathymetry are evident. Firstly, a DTM-W enables the creation of hydrodynamic models, with Topo-bathy LiDAR proving to be a highly effective method. Secondly, the detailed bathymetric data reveals terrain features which alter the flow of water. This is a significant enhancement over DTMs that lack bathymetric information.

Thirdly, the lower flying altitude and strategic flight paths of the ULS, resulted in a more detailed representation of the full environment compared to the ALS DTM. This is made possible by the ULS point cloud's ~10 cm spatial resolution - approximately six times greater than ALS - leading to fewer occlusions and a more complete representation of the bathymetric environment.

Finally, as Topo-bathy LiDAR can penetrate vegetation, the ULS DTM produced a more comprehensive dataset and was less affected by vegetation than ALS data, largely due to its lower flying altitude. However, the ALS System's broader survey allowed greater spatial coverage, where the ULS survey was limited to a focused region.

Further investigations will be made into utilising the full Topo-bathy ALS point cloud. Areas of vegetation and occlusions will also be investigated to determine a suitable method for post-processing. Considerations and adaptations to the workflow will be considered to produce a streamlined methodology.

Acknowledgements

This work is funded by Centre for Doctoral Training for Resilient Flood Futures, primarily invested by the Natural Environment Research Council: NE/Y006364/1. Fieldwork was undertaken by TU Wien within the transnational WEAVE projects PhotoBathyWave and BathyNerf funded by the Austrian Science Fund (FWF) and the German Research Foundation (DFG). PhotobathyWave: I 5935-N (FWF), 496002628 (DFG); BathyNerf: PIN1353223 (FWF), JU 2847/2-1 (DFG). Special thanks to the Photogrammetry department at TU Wien for collaborating and to Jan Rhomberg-Kauert and Johannes Otepka of TU Wien for ongoing OPALS support and advice.

References

Bangen, S.G., Wheaton, J.M., Bouwes, N., Bouwes, B., Jordan, C., 2014. A methodological intercomparison of topographic

survey techniques for characterizing wadeable streams and rivers. *Geomorphology* 206, 343–361. <https://doi.org/10.1016/j.geomorph.2013.10.010>

Blöschl, G., 2024. September 2024 flooding in Central Europe: The Austrian experience. *EGU Blogs, GeoLog*. URL <https://blogs.egu.eu/geolog/2024/09/26/september-2024-flooding-in-central-europe-the-austrian-experience/> (accessed 3.10.25).

Brasington, J., Langham, J., Rumsby, B., 2003. Methodological sensitivity of morphometric estimates of coarse fluvial sediment transport. *Geomorphology* 53, 299–316. [https://doi.org/10.1016/S0169-555X\(02\)00320-3](https://doi.org/10.1016/S0169-555X(02)00320-3)

Chow, V.T., 2009. *Open-channel hydraulics*. Blackburn Press, Caldwell, NJ.

Chow, V.T., Maidment, D.R., Mays, L.W., 1988. *Applied hydrology*, McGraw-Hill series in water resources and environmental engineering. McGraw-Hill, New York St. Louis Paris [etc.].

Cook, A., Merwade, V., 2009. Effect of topographic data, geometric configuration and modeling approach on flood inundation mapping. *Journal of Hydrology* 377, 131–142. <https://doi.org/10.1016/j.jhydrol.2009.08.015>

D. L. Brakensiek, R. L. Engleman, W. J. Rawls, 1981. Variation within Texture Classes of Soil Water Parameters. *Transactions of the ASAE* 24, 0335–0339. <https://doi.org/10.13031/2013.34253>

ECMWF, 2024. Storm Boris and European flooding September 2024 [WWW Document]. ECMWF. URL <https://www.ecmwf.int/en/about/media-centre/focus/2024/storm-boris-and-european-flooding-september-2024> (accessed 3.10.25).

European Union Aviation Safety Agency, 2024. *Easy Access Rules for Unmanned Aircraft Systems (1)*. EASA.

Frizzle, C., Trudel, M., Daniel, S., Pruneau, A., Noman, J., 2024. LiDAR topo-bathymetry for riverbed elevation assessment: A review of approaches and performance for hydrodynamic modelling of flood plains. *Earth Surf Processes Landf* 49, 2585–2600. <https://doi.org/10.1002/esp.5808>

Glenis, V., Kutija, V., Kilsby, C.G., 2018. A fully hydrodynamic urban flood modelling system representing buildings, green space and interventions. *Environmental Modelling & Software* 109, 272–292. <https://doi.org/10.1016/j.envsoft.2018.07.018>

Glira, P., Pfeifer, N., Briese, C., Ressler, C., 2015. A Correspondence Framework for ALS Strip Adjustments based on Variants of the ICP Algorithm. *pfg* 2015, 275–289. <https://doi.org/10.1127/pfg/2015/0270>

Glira, P., Pfeifer, N., Mandlburger, G., 2016. Rigorous Strip Adjustment of UAV-based Laserscanning Data Including Time-Dependent Correction of Trajectory Errors. *Photogram Engng Rem Sens* 82, 945–954. <https://doi.org/10.14358/PERS.82.12.945>

Grimaldi, S., Li, Y., Walker, J.P., Pauwels, V.R.N., 2018. Effective Representation of River Geometry in Hydraulic Flood

- Forecast Models. *Water Resources Research* 54, 1031–1057. <https://doi.org/10.1002/2017WR021765>
- Guo, K., Guan, M., Yu, D., 2021. Urban surface water flood modelling – a comprehensive review of current models and future challenges. *Hydrol. Earth Syst. Sci.* 25, 2843–2860. <https://doi.org/10.5194/hess-25-2843-2021>
- Horritt, M.S., Bates, P.D., 2002. Evaluation of 1D and 2D numerical models for predicting river flood inundation. *Journal of Hydrology* 268, 87–99. [https://doi.org/10.1016/S0022-1694\(02\)00121-X](https://doi.org/10.1016/S0022-1694(02)00121-X)
- Iliadis, C., Galiatsatou, P., Glenis, V., Prinos, P., Kilsby, C., 2023. Urban Flood Modelling under Extreme Rainfall Conditions for Building-Level Flood Exposure Analysis. *Hydrology* 10, 172. <https://doi.org/10.3390/hydrology10080172>
- Janowski, Ł., Skarlatos, D., Agraftiotis, P., Tysi c, P., Pydyn, A., Popek, M., Kotarba-Morley, A.M., Mandlburger, G., Gajewski, Ł., Ko akowski, M., Papadaki, A., Gajewski, J., 2024. High resolution optical and acoustic remote sensing datasets of the Puck Lagoon. *Sci Data* 11, 360. <https://doi.org/10.1038/s41597-024-03199-y>
- Kasvi, E., Salmela, J., Lotsari, E., Kumpula, T., Lane, S.N., 2019. Comparison of remote sensing based approaches for mapping bathymetry of shallow, clear water rivers. *Geomorphology* 333, 180–197. <https://doi.org/10.1016/j.geomorph.2019.02.017>
- Kraus, K., Pfeifer, N., 1998. Determination of terrain models in wooded areas with airborne laser scanner data. *ISPRS Journal of Photogrammetry and Remote Sensing* 53, 193–203. [https://doi.org/10.1016/S0924-2716\(98\)00009-4](https://doi.org/10.1016/S0924-2716(98)00009-4)
- Mandlburger, G., Hauer, C., Wieser, M., Pfeifer, N., 2015. Topo-Bathymetric LiDAR for Monitoring River Morphodynamics and Instream Habitats—A Case Study at the Pielach River. *Remote Sensing* 7, 6160–6195. <https://doi.org/10.3390/rs70506160>
- Mandlburger, G., Pfennigbauer, M., Pfeifer, N., 2013. Analyzing near water surface penetration in laser bathymetry – A case study at the River Pielach. *ISPRS Ann. Photogramm. Remote Sens. Spatial Inf. Sci.* II-5/W2, 175–180. <https://doi.org/10.5194/isprsannals-II-5-W2-175-2013>
- Mandlburger, G., Pfennigbauer, M., Schwarz, R., Fl ry, S., Nussbaumer, L., 2020. Concept and Performance Evaluation of a Novel UAV-Borne Topo-Bathymetric LiDAR Sensor. *Remote Sensing* 12, 986. <https://doi.org/10.3390/rs12060986>
- Mandlburger, G., Pfennigbauer, M., Wieser, M., Riegl, U., Pfeifer, N., 2016. EVALUATION OF A NOVEL UAV-BORNE TOPO-BATHYMETRIC LASER PROFILER. *Int. Arch. Photogramm. Remote Sens. Spatial Inf. Sci.* XLI-B1, 933–939. <https://doi.org/10.5194/isprsarchives-XLI-B1-933-2016>
- Mandlburger, G., Rhomberg-Kauert, J., Gueguen, L.-A., Muslow, C., Brezovsky, M., Dammert, L., Haines, J., Glas, S., Himmelsbach, T., Schulte, F., Amon, P., Winiwarter, L., Jutzi, B., Maas, H.-G., 2025. Mapping shallow inland running waters with UAV-borne photo and laser bathymetry. *Hydrographische Nachrichten* 42–54. <https://doi.org/10.23784/HN130-06>
- McKean, J., Tonina, D., Bohn, C., Wright, C.W., 2014. Effects of bathymetric lidar errors on flow properties predicted with a multi-dimensional hydraulic model: Lidar bathymetry and hydraulic models. *J. Geophys. Res. Earth Surf.* 119, 644–664. <https://doi.org/10.1002/2013jf002897>
- Opals, 2025. Python script opalsQuality [WWW Document]. Orientation and Processing of Airborne Laser Scanning data. URL <https://opals.geo.tuwien.ac.at/html/nightly/opalsQuality.html> (accessed 5.25.25).
- Overture Maps Foundation, 2024. Who We Are [WWW Document]. Who we are. URL <https://overturemaps.org/about/who-we-are/> (accessed 5.9.25).
- Pfeifer, N., Mandlburger, G., Otepka, J., Karel, W., 2014. OPALS – A framework for Airborne Laser Scanning data analysis. *Computers, Environment and Urban Systems* 45, 125–136. <https://doi.org/10.1016/j.compenvurbsys.2013.11.002>
- Rawls, W.J., Brakensiek, D.L., Miller, N., 1983. Green-ampt Infiltration Parameters from Soils Data. *J. Hydraul. Eng.* 109, 62–70. [https://doi.org/10.1061/\(ASCE\)0733-9429\(1983\)109:1\(62\)](https://doi.org/10.1061/(ASCE)0733-9429(1983)109:1(62))
- RIEGL Laser Measurement Systems, 2025. Reigl VQ-880-GII Datasheet 2025-03-03 (Datasheet).
- RIEGL Laser Measurement Systems, 2024. Riegl VQ-840-GL Datasheet 2024-10-09.
- Shan, J., Toth, C.K., 2018. Topographic laser ranging and scanning: principles and processing, Second edition. ed. CRC Press, Boca Raton, FL.
- The European Space Agency, 2025. Introducing Sentinel-2. Introducing Sentinel-2. URL https://www.esa.int/Applications/Observing_the_Earth/Copernicus/Sentinel-2/Introducing_Sentinel-2 (accessed 5.9.25).
- Tomsett, C., Leyland, J., 2019. Remote sensing of river corridors: A review of current trends and future directions. *River Research & Apps* 35, 779–803. <https://doi.org/10.1002/rra.3479>
- Wieser, M., Hollaus, M., Mandlburger, G., Glira, P., Pfeifer, N., 2016. ULS LiDAR SUPPORTED ANALYSES OF LASER BEAM PENETRATION FROM DIFFERENT ALS SYSTEMS INTO VEGETATION. *ISPRS Ann. Photogramm. Remote Sens. Spatial Inf. Sci.* III-3, 233–239. <https://doi.org/10.5194/isprsannals-III-3-233-2016>
- Wimmer, M.H., Mandlburger, G., Ressler, C., Pfeifer, N., 2024. Strip Adjustment of Multi-Temporal LiDAR Data—A Case Study at the Pielach River. *Remote Sensing* 16, 2838. <https://doi.org/10.3390/rs16152838>
- Woodget, A.S., Carbonneau, P.E., Visser, F., Maddock, I.P., 2015. Quantifying submerged fluvial topography using hyperspatial resolution UAS imagery and structure from motion photogrammetry. *Earth Surf Processes Landf* 40, 47–64. <https://doi.org/10.1002/esp.3613>